Electronic Supplementary Material (ESI) for Biomaterials Science.
This journal is © The Royal Society of Chemistry 2022

Supporting Information

Subcutaneous delivery of an antibody against SARS-CoV-2 from a supramolecular hydrogel depot

Catherine M. Kasse,[a] Anthony C. Yu,[a] Abigail E. Powell,[b,c] Gillie A. Roth,[d] Celine S. Liong,[d] Carolyn K. Jons,[a] Awua Buahin,[a] Caitlin L. Maikawa,[d] Xueting Zhou,[d] Sawsan Youssef,[e] Jacob E. Glanville,[e] Eric A. Appel[a,c,d,f,g,h,*]

[a] Department of Materials Science and Engineering, Stanford University, Stanford, CA 94305, USA

[b] Department of Biochemistry, Stanford University School of Medicine, Stanford, CA 94305, USA

[c] Stanford CHEM-H, Stanford University Stanford, CA 94305, USA

[d] Department of Bioengineering, Stanford University, Stanford, CA 94305, USA

[e] Centivax Inc. South San Francisco, CA 94080, USA

[f] Institute for Immunity, Transplantation, and Infection, Stanford University School of Medicine, Stanford, CA 94305, USA

[g] Department of Pediatrics - Endocrinology, Stanford University School of Medicine Stanford, CA 94305, USA

[h] Stanford Woods Institute for the Environment, Stanford University Stanford, CA 94305, USA

[*]To whom correspondence should be addressed; E-mail: eappel@stanford.edu.

Contents

1 Supplemental Methods

1.1 Formulation and in vivo pharmacokinetic study of Centi-C10 antibody in histidine buffer

Prior to hydrogel formulation, the Centi-C10 antibody was buffer exchanged from PBS into 25 mM histidine buffer (pH 6) (sterile, Bioworld) with 150 mM USP-grade sucrose (Sigma-Aldrich) using spin desalting columns. Hydrogel stock solution components were prepared in the same histidine buffer, and the hydrogels were formulated as described in the paper. The in vivo pharmacokinetic study was conducted as described in the paper.

1.2 Histology sample preparation

A parallel cohort of mice (n=3) to the PK study were subcutaneously administered both unloaded hydrogel and hydrogel loaded with Centi-C10 antibody on separate flanks. At day 7, the mice were euthanized and the hydrogel and surrounding subcutaneous tissue were excised, embedded in OCT (optimal cutting temperature) medium in block molds, and flash frozen with liquid nitrogen. Frozen samples were submitted to Stanford Animal Histology Services for sectioning, mounting, and standard staining.

1.3 In vivo PNP hydrogel biocompatibility in rats

Female Wistar rats were used to assess the biocompatibility of the PNP hydrogel (n=3/group). Rats were sedated under isoflurane anesthesia to allow for surgical administration of 800 μl of 1:10 PNP hydrogel to the peritoneal cavity. Four weeks post-administration, the rats were submitted for blood chemistry analysis. This animal study was performed in accordance with National Institutes of Health guidelines and with the approval of the Stanford Administrative Panel on Laboratory Animal Care (APLAC-33032).

1.4 Pharmacokinetic modeling

1.4.1 One compartment model

The differential equations and the analytical solution for a standard one compartment pharmacokinetic model with first order reaction kinetics are described in Zou, et al.[1] Briefly, the form of the analytical solution of the single compartment model for drug serum concentration as a function of time, $C(t)$, used in our modeling is as follows:

$$C(t) = \frac{F k_{abs} M_0}{V_d (k_{abs} - k_{elim})} \left(e^{-k_{elim} t} - e^{-k_{abs} t} \right) \tag{S1}$$

where F = bioavailability, k_{abs} = rate constant of absorbance from subcutaneous space into the bloodstream, M_0 = initial dose of drug, V_d = volume of distribution, k_{elim} = rate constant of drug elimination, and t = time.

1.4.2 Two compartment model

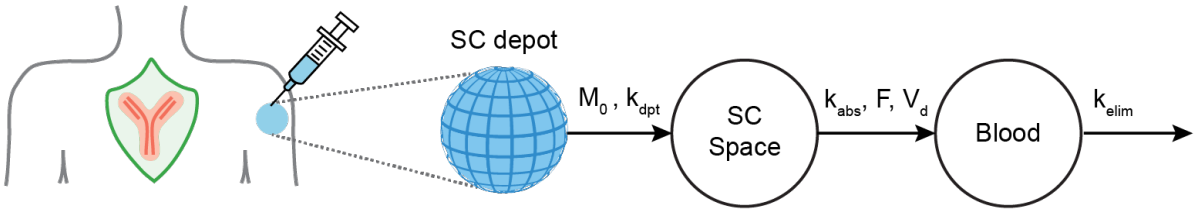

Figure S1: Two compartment model schema

The following differential equations and initial conditions were written to describe the mass transport depicted in Figure S1, where M_1 refers to drug mass in the subcutaneous hydrogel depot compartment, M_2 refers to drug mass in the subcutaneous compartment, and M_3 refers drug mass in the blood serum compartment:

$$\frac{dM_1(t)}{dt} = -k_{dpt}M_1(t), \quad M_1(0) = M_0 \tag{S2}$$

$$\frac{dM_2(t)}{dt} = k_{dpt}M_1(t) - k_{abs}M_2(t), \quad M_2(0) = 0 \tag{S3}$$

$$\frac{dM_3(t)}{dt} = k_{abs}FM_2(t) - k_{elim}M_3(t), \quad M_3(0) = 0 \tag{S4}$$

where k_{dpt} = rate constant of drug release from hydrogel depot, and

$$C(t) = \frac{M_3(t)}{V_d} \tag{S5}$$

These equations and conditions were solved for the following analytical solution:

$$C(t) = \frac{M_0 F k_{dpt} k_{abs} e^{-k_{elim}t}}{V_d(k_{dpt} - k_{abs})(k_{elim} - k_{dpt})(k_{elim} - k_{abs})} \left[(k_{elim} - k_{dpt})e^{(k_{elim}-k_{abs})t} + (k_{abs} - k_{elim})e^{(k_{elim}-k_{dpt})t} + k_{dpt} - k_{abs}\right] \tag{S6}$$

1.5 CryoTEM sample preparation and imaging

For cryogenic transmission electron microscopy (CryoTEM) grid preparation, a glow-discharged R1.2/1.3 Quantifoil grid or a lacey carbon grid was dipped into the sample to pick up some sample, and a Vitrobot Mark IV (Thermo Fisher Scientific, USA) was used to plunge grids into liquid ethane to form vitreous ice. CryoTEM images were collected using Thermo Fisher Talos Arctica Cryo-TEM (Thermo Fisher Scientific, USA) equipped with a K3 direct electron detector and an accelerated voltage of 200 kV. Micrographs were collected at 79000x magnification (pixel size 1.11 Å/pixel) at -3.0 μm defocus. The total electron dose was 36 e-/Å^2.

2 Centi-C10 antibody sequence

VH

QVQLVQSGAEVKKPGSSVKVSCKASGYPFTNYGISWVRQAPGQGLEWMGWMNPNSGNTGYAQKFQ
GRVTITADESTSTAYMELSSLRSEDTAVYYCATLSGISTPMDVWGQGTLVTVSS

VL

DIVMTQSPDSLAVSLGERATINCRSSQSVLYSSNNKNYFAWYQQKPGQPPKLLIYWASIRGSGVPDRFSGS
GSGTDFTLTISSLQAEDVAVYYCHQYYTTPPTFGGGTKVEIKR

3 Additional PNP hydrogel rheology

3.1 Rheological stability

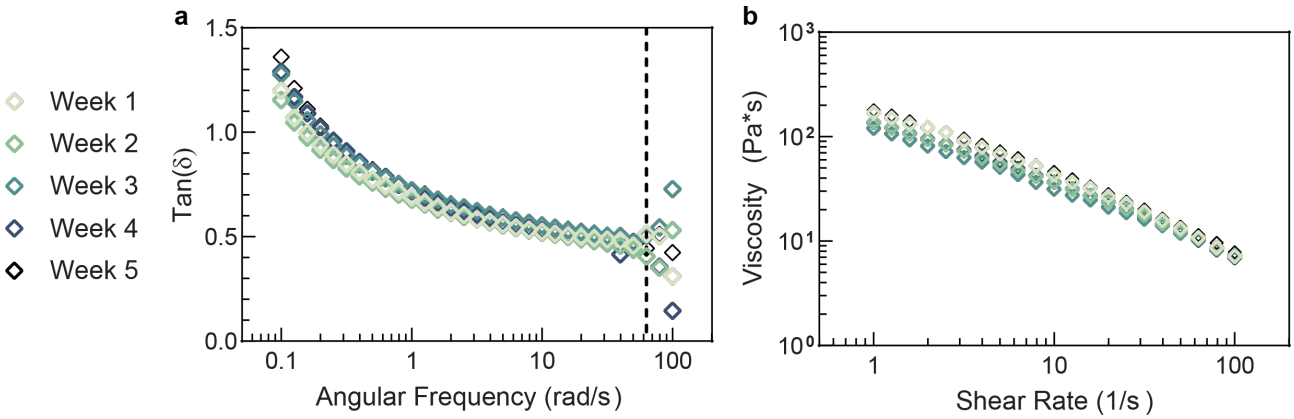

Figure S 2: Relative elasticity and steady shear measurements. (a) Tan(δ) for the high concentration gel measured once every week for 5 weeks illustrates minimal change in relative elasticity. The dotted line indicates the angular frequency cutoff, where higher values are likely influenced by inertial effects. (b) Steady shear measurements of the high concentration gel measured once every week for 5 weeks illustrates minimal change in viscosity or shear-thinning index.

3.2 Viscosity recovery time from step shear test

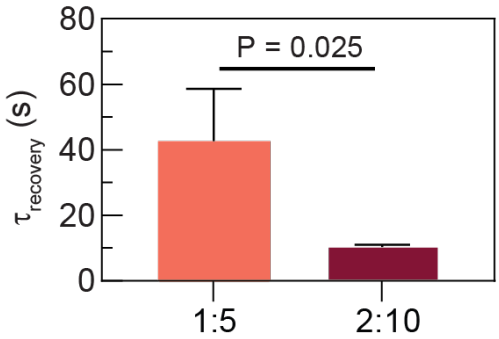

Figure S 3: Characteristic recovery time τ was determined from the viscosity recovery curves from the step shear tests shown in Figure 2d (mean $\pm$ SD, n=3, final three cycles); p-value determined by two-sided, unpaired t-test.

4 Fluorescence recovery after photobleaching (FRAP) data

Table S1. Diffusivity values as determined by FRAP. Mean ±SD (n=3)

Gel formulation	D_{IgG} ($\mu m^2/s$)	$D_{polymer}$ ($\mu m^2/s$)	$D_{IgG}/D_{polymer}$
1:5	4.3 ±0.4	1.3 ±0.2	3.4 ±0.7
2:10	0.9 ±0.2	1.4 ±0.1	0.6 ±0.1

5 In vitro Centi-C10 stability at 50 °C

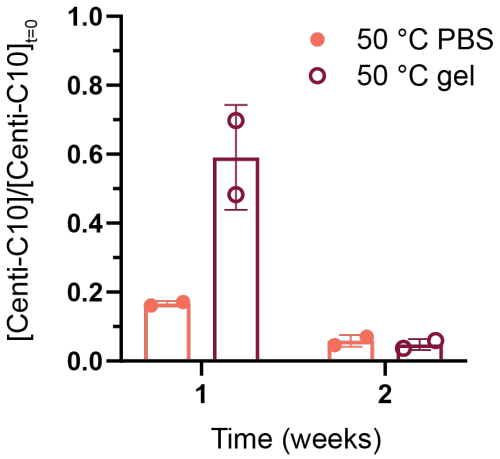

Figure S4: In vitro stability of Centi-C10 in PBS buffer formulation compared to hydrogel encapsulated Centi-C10 at 50 °C quantified via anti-RBD ELISA (mean ± SD, assayed in duplicate)

6 In vivo PK data for Centi-C10 antibody in hydrogel with histidine buffer

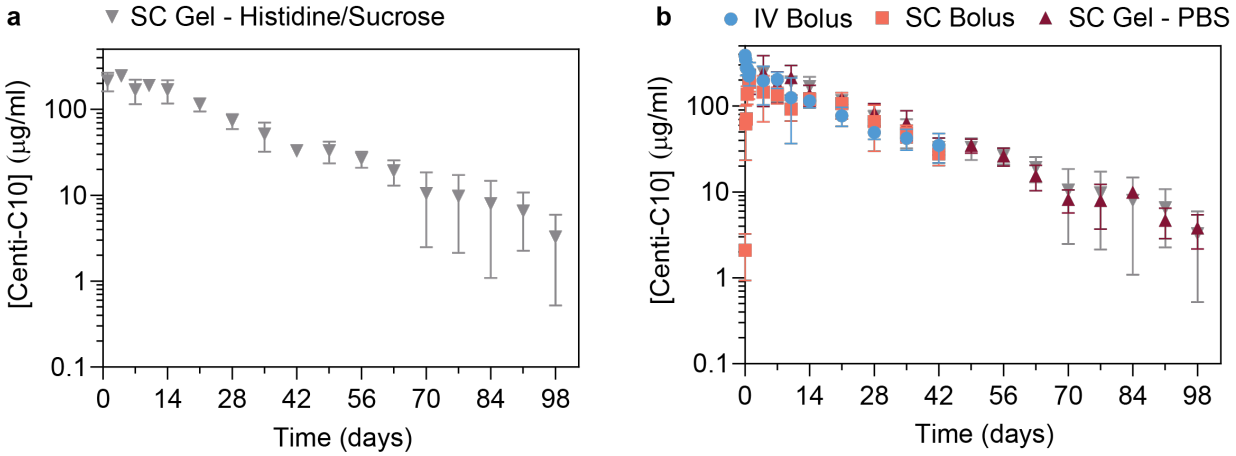

Figure S5: Centi-C10 serum pharmacokinetics in a preclinical mouse model as determined by ELISA. a) PK profile for Centi-C10 administered from a SC gel with histidine/sucrose buffer. b) SC gel with histidine/sucrose buffer overlaid with IV, SC bolus, and SC gel with PBS as shown in the paper. Data points shown as mean $\pm$ SD (n = 3 prior to 24 hrs, otherwise n = 6; for gel groups, n $\geq$ 4 after day 63).

7 Biocompatibility

7.1 Histology - Day 7

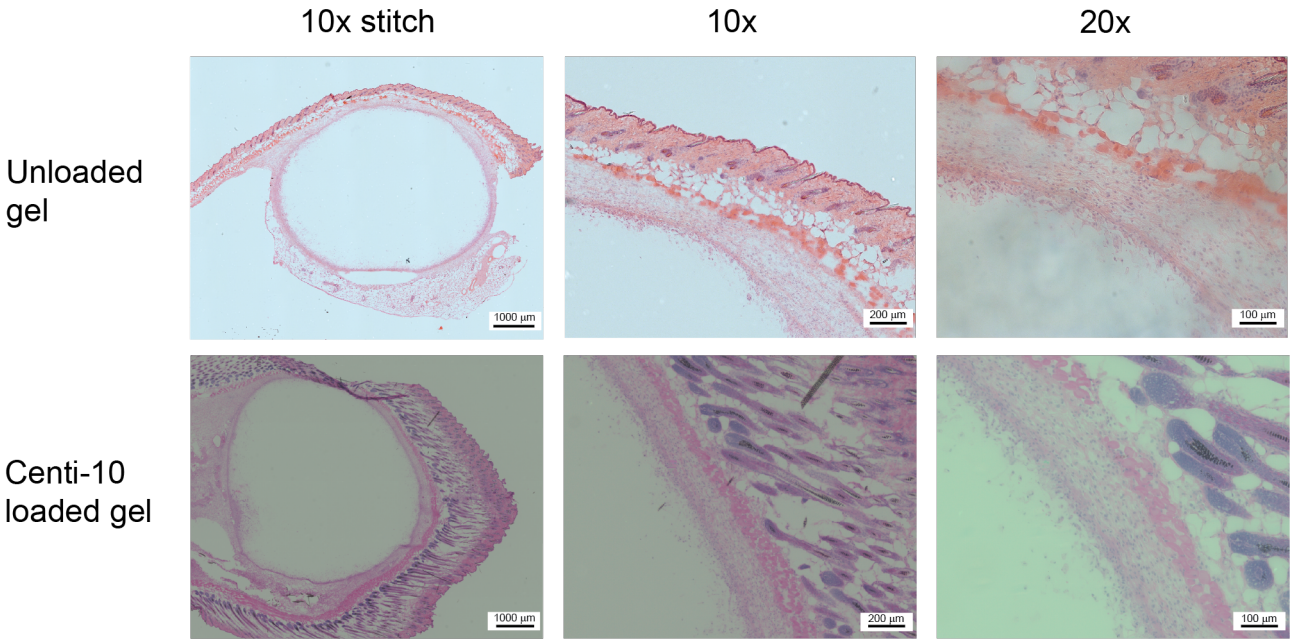

Figure S6: Hematoxylin and eosin (H & E) staining, representative images at Day 7. Stitched image show entire cross section of excised hydrogel along with surrounding skin tissue.

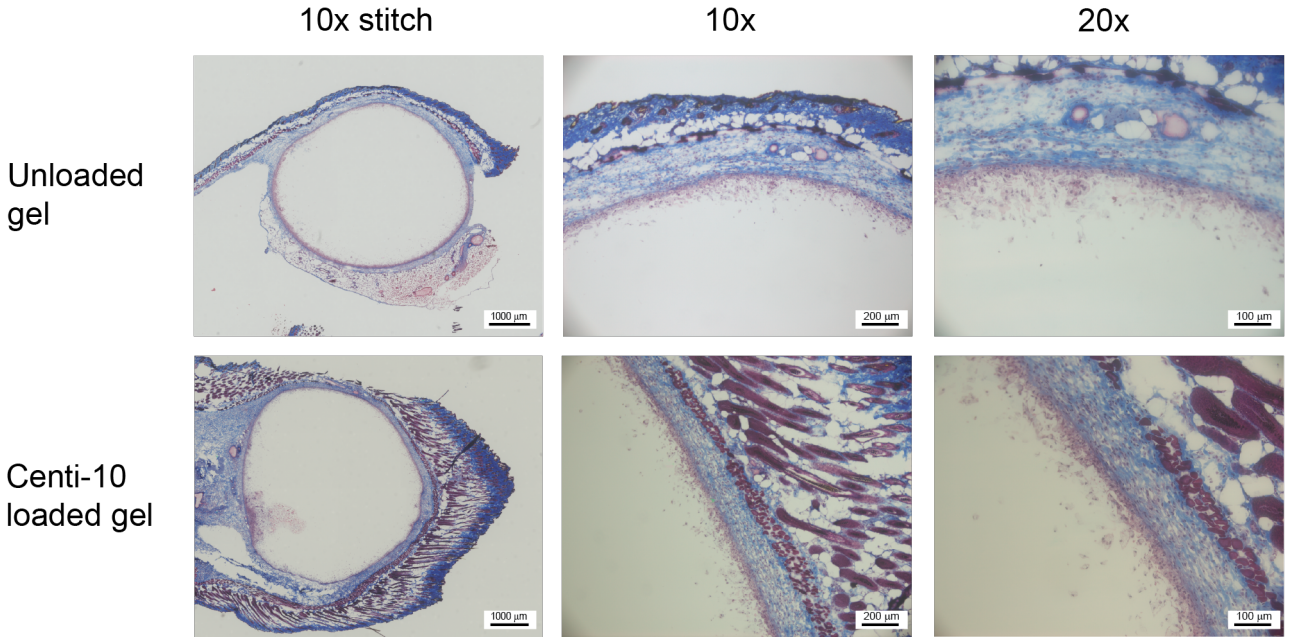

Figure S7: Trichrome staining, representative images at Day 7. Stitched image show entire cross section of excised hydrogel along with surrounding skin tissue.

7.2 Blood chemistry

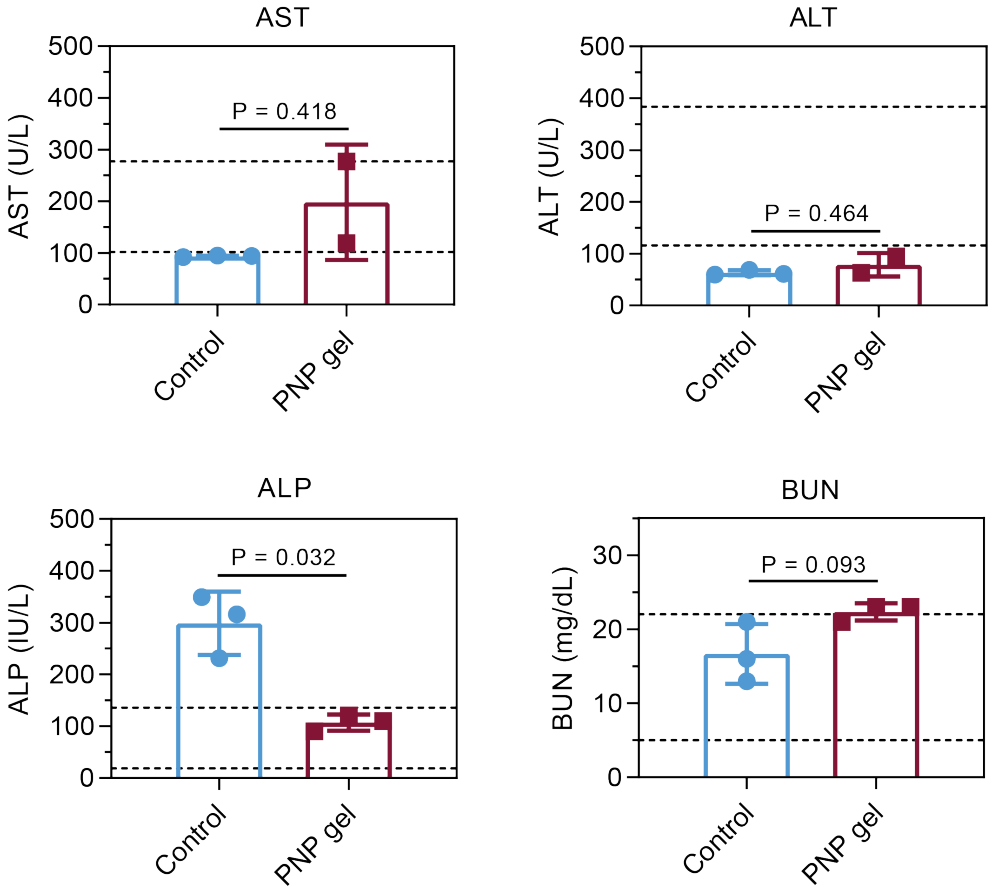

Figure S8: Blood chemistry analysis 4 weeks post-administration of PNP hydrogel in the peritoneal space of rats (mean ± SD, n=3 mice/group); p-values determined by paired t-test. Control animals were administered saline via intraperitoneal injection. Dotted lines indicate the normal range for respective markers, determined as the mean ± two standard deviations for concentrations exhibited in healthy Wistar rats.

8 Modeling depot drug release as a function of cargo diffusivity

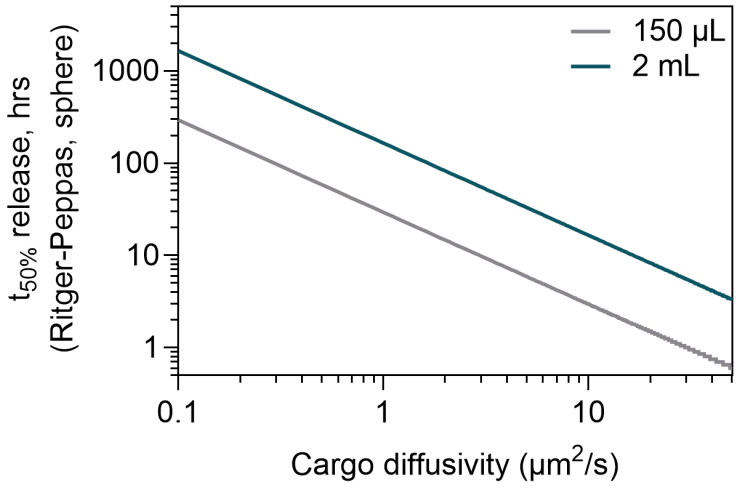

Figure S9: Time to 50% release from a depot as a function of encapsulated cargo diffusivity from a 150 μL depot (mouse) and a 2 mL depot (human), which are typical volumes for subcutaneous injection. Profiles generated in Matlab using the Ritger-Peppas mass release approximation assuming Fickian release and spherical depot.[2]

9 CryoTEM images of PNP hydrogels

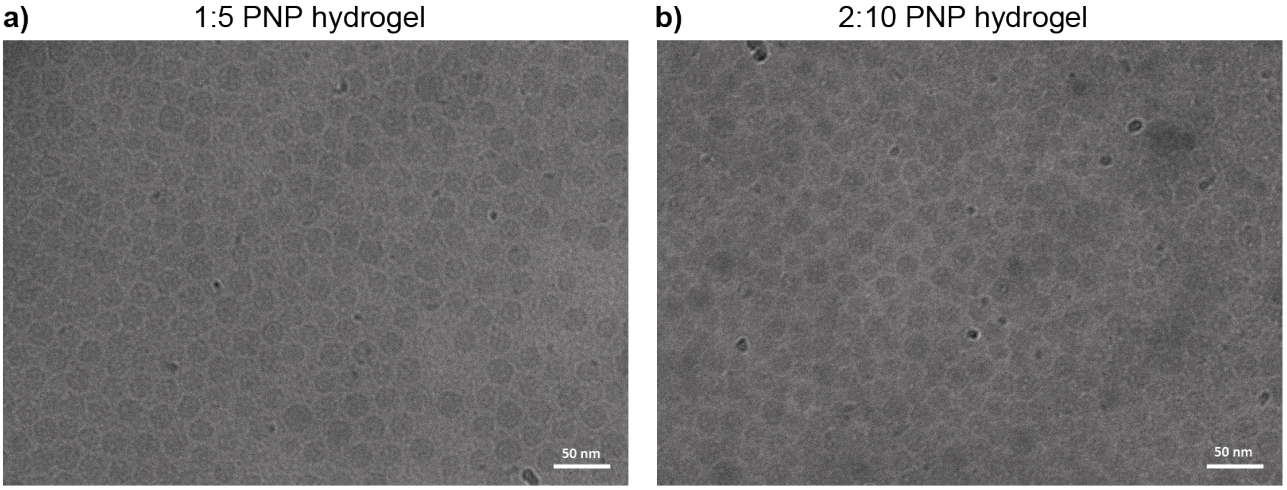

Figure S10: CryoTEM images of PNP hydrogels showing nanoparticles are evenly dispersed in the polymer matrix and not agglomerated. Scale bar 50 nm.

References

[1] Zou, H.; Banerjee, P.; Leung, S. S. Y.; Yan, X. *Frontiers in Pharmacology* **2020**, *11*, 997.

[2] Ritger, P. L.; Peppas, N. A. *Journal of controlled release* **1987**, *5*, 37–42.